Inversion-based Precision-Positioning of Switching Inertial Reaction Devices

Clint Vander Giessen† Qingze Zou† Santosh Devasia§
Mechanical Engineering Department, Box 352600, Univ. of Washington, Seattle, WA, 98195

***Abstract*— Inertial reaction devices enable nano/micro resolution positioning over macroscopic ranges. Such positioning devices are characterized by the displacement of a mass by utilizing stick-slip phenomena between the mass and the device's actuators. The displacement of the actuator (i.e., the driving waveform) is chosen such that the mass sticks to the actuator and is displaced with the actuator during the first *tracking* phase, and the mass slips over the actuator during the second *retrace* phase such that the position of the actuator is reset. However, as the frequency of the driving waveform is increased, vibrations are induced in the actuators, preventing precise actuator positioning and thereby, limiting the maximum achievable operating speed. In this paper, we employ an inversion-based method to allow the actuators to track high-frequency driving waveforms without exciting the vibrations, therefore achieving high-speed operation of the inertial reaction device. Experimental results on a one-degree-of freedom inertial reaction rotational device showed that the operating speed can be substantially increased (more than doubled) by using the proposed method.**

I. Introduction

Inertial reaction (also referred to as impact drive, or slip stick) devices are characterized by the displacement of a mass by utilizing the stick-slip phenomena between the mass and the device's actuators. The idea of moving objects using the stick-slip phenomena was used to design a one degree-of-freedom (DOF) inertial reaction device by Pohl [1]; then Niedermann *et. al*. [2] modified the design to obtain unlimited translation range. Briefly, the operation of inertial reaction devices consists of two parts: (i) the tracking phase and (ii) the retrace phase, as shown in Fig. 1. During the first tracking phase, the mass sticks to the actuator (due to static friction) and the actuator applies force on the mass. Then, during the second retrace phase, the actuator retracts quickly such that the inertial force of the mass overcomes the static friction and the mass slips with respect to the actuator — therefore, the mass continues to move while the actuator moves in the opposite direction to reset its position. Because of the precision positioning achieved by the actuator made from piezomaterial, the mass can be positioned with nanometer resolution. Therefore, by periodically repeating this two-phase driving waveform, the mass can be moved in nano/micro steps (i.e., with high resolution) over large ranges. Such inertial reaction devices have been successfully used for: (1) high-resolution large-range positioning in scanning probe microscopy (SPM) [3-6]; (2) alignment of optical components using three DOF rotational devices [7]; (3) material handling in nanolithography [8]; and (4) robotic actuation in micro- and nanofabrication [9].

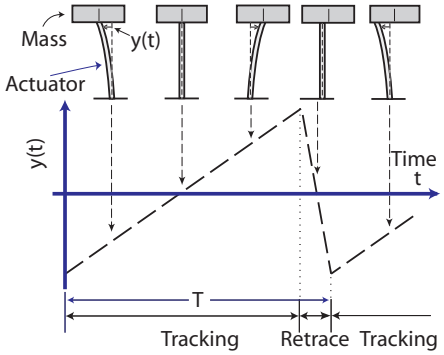

Fig. 1. The schematic motion of the inertial reaction device, which includes the tracking phase and the retrace phase, where $y(t)$ is the actuator deflection and T is the period of the driving waveform.

A problem with inertial-reaction devices is that the operating speed is limited by the induced mechanical vibrations of the actuator. As the frequency of the driving waveform, $f = 1/T$ (where T is the period of the driving waveform as shown in Fig. 1), increases, the dynamics of the actuator can be excited, generating the induced vibrations in the actuator. These induced vibrations (if not compensated-for) prevent the inertial mass from sticking to the actuator during the tracking phase, resulting in reduction of the desired displacement (of the mass). Thereby, the induced vibrations limit the maximum achievable operating speed [10]. When the waveform frequency is sufficiently high, vibrations dominate the actuator displacement and mass can no longer stick to the actuator during the tracking phase – the mass is floating and can move in the reverse direction [5]. Thus, the dynamics-induced vibrations in the actuator displacement must be compensated-for to achieve high speed operation of inertial reaction devices [10].

Current approaches used in inertial reaction devices cannot achieve high-speed operation because they do not account-for the vibrational dynamics of the actuator. In current applications, the input to the actuator is obtained simply by scaling the desired displacement trajectory $y_d(t)$ with the *DC-Gain* of the actuator [10]:

$$u(t) = \frac{1}{K_{dc}} y_d(t). \qquad (1)$$

† Clint Vander Giessen is currently with Electro Scientific Industries Inc., Portland, OR, 97229.
‡ E-mail:qzouatuw@u.washington.edu
§ E-mail: devasia@u.washington.edu

where K_{dc} is the DC-gain (static sensitivity) of the actuator. Such a control scheme (hereafter referred to as the *DC-gain* approach) does not consider the actuator dynamics, and is applicable only when the driving-waveform frequencies are significantly smaller than the first resonant frequency of the actuator– as the driving-waveform frequency becomes close to the first resonant frequency of the actuator, the dynamics of the actuator can be excited by the *DC-Gain* input and leads to the induced mechanical vibrations in the actuator, limiting the high-speed performance. One way to alleviate the vibration problem is to choose actuators with resonant frequencies significantly higher than the desired driving waveform frequency [6]. However, a problem with choosing such high-frequency actuators is that, in general, an actuator with a higher resonant frequency also tends to be stiffer and therefore tends to have a smaller displacement range. Thus, even though the use of high-resonant-frequency actuators allows for higher driving waveform frequencies, it will also lead to substantially decreased movement of the mass during each step — this decreased step size again limits the maximum operating speed.

In this article, we use an inversion-based method [11-13] to improve the operation speed of the inertial reaction devices. In this approach, the input (called *inverse input* is obtained by passing the desired trajectory through the inverse of the actuator dynamics such that exact tracking can be achieved when this inverse input is applied. The proposed method is illustrated by applying it to an inertial-reaction rotational device in both simulations and experiments. The simulation and experimental results are presented to show that the operating speed can be increased more than twice by using the proposed inversion-based method.

The rest of the article is in the following format. The inertial reaction device is described in Sec. II along with the implementation of the proposed inversion-based approach for output-tracking. In Sec. III, this inversion-based output tracking technique is applied to the inertial reaction device, and the discussion of the simulation and experimental results are presented. Our conclusions are in Sec. IV.

II. Inversion-based Dynamics Compensation

In this section, we describe the implementation of the inversion-based method [11], [13] to inertial reaction devices. We start with describing the inertial reaction device studied in this article and its dynamics model.

A. System Description and Modeling

The experimental inertial reaction device studied in this article utilizes three piezoceramic bimorph actuators mounted at 120° angles from each other as shown in Fig. 2. A steel ball was attached to the top of each actuator and a glass disk was placed on the steel balls yielding a kinematic seat, allowing the disk to be in continuous contact with each actuator. The disk was centered using a sapphire vee bearing mounted to the disk and a needle positioned in the sapphire bearing; the needle is held in place by a cantilever arm. The piezoceramic actuators were configured such that the applied voltage leads to a tip displacement (top of the actuator in Fig. 2) in the same tangential direction for all three actuators — in this application, the same voltage was simultaneously applied to all the three actuators.

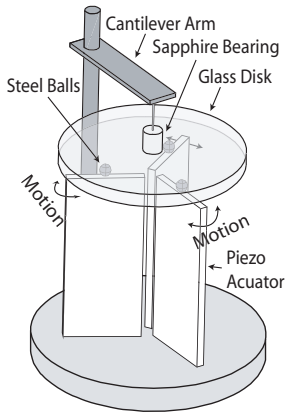

Fig. 2. Experimental inertial reaction device.

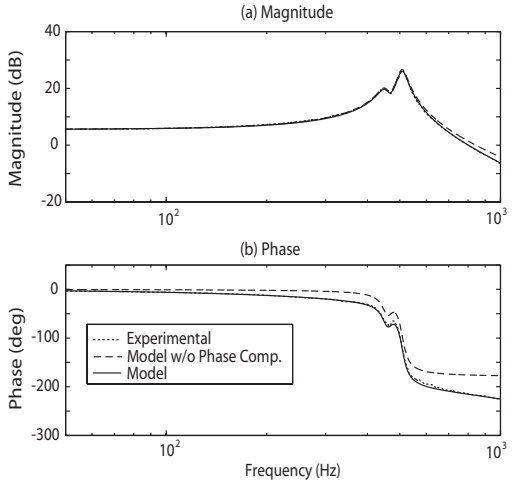

Fig. 3. The frequency response of the piezo actuator measured experimentally (dotted line), the lower-order model without phase compensation (dashed line) and the higher-order model with phase compensation (solid line).

The Model An empirical dynamic model of the system's actuators was obtained using a dynamic signal analyzer (DSA). A sinusoidal input voltage $u(t)$ generated by the DSA is applied to the actuator and the position of the actuator $y(t)$ is measured (by using an inductive sensor) and fed back to the DSA. The measured frequency response is shown in Fig. 3, which is used to model the system dynamics as the following transfer function from the input voltage $U(s)$ $(Volt)$ to the actuator-tip displacement $Y(s)$ (μm):

$$\hat{G}(s) = \frac{Y(s)}{U(s)} = \frac{K \times \prod_{j=1}^{4}(s - z_j)}{\prod_{i=1}^{6}(s - p_i)} \qquad (2)$$

where $U(s)$ and $Y(s)$ are the Laplace transforms of $u(t)$ and $y(t)$ respectively, the unit of the Laplace variable s is scaled to rad/ms to reduce potential computational errors, the gain $K = 0.2173$, and the zeros z_j $(j = 1, \cdots, 4)$ and the poles p_i $(i = 1, \cdots, 6)$ given in Table I.

TABLE I

ZEROS AND POLES OF THE MODEL AND THEIR CORRESPONDING FREQUENCY $f_q = \frac{1}{2\pi}\sqrt{Re[q]^2 + Im[q]^2}$ (kHz), WHERE q IS A SYSTEM POLE OR ZERO.

	Zeros	Freq. (kHz)
$z_{1,2}$	$-.1184 \pm j2.9233$	.466
z_3	-94.248	15.00
z_4	-94.248	15.00
	Poles	**Freq. (kHz)**
$p_{1,2}$	$-.1209 \pm j2.8495$	.454
$p_{3,4}$	$-.1097 \pm j3.1888$	.508
p_5	-11.938	1.900
p_6	-11.938	1.900

Modeling the Phase of the Transfer Function Note that a pair of zeros (z_3 and z_4 in Table I) at 15 KHz and a pair of poles (p_5 and p_6 in Table I) at 1.9 KHz in the transfer function $\hat{G}(s)$ are present in the model — these are located beyond the measured frequency range of 1 KHz (see Fig. 3 and Table I). These two pairs of zeros and poles are added to compensate for the effect of the unmodeled vibrational modes outside the measured frequency range (e.g., [14], [15]). As shown in Fig. 3 (dashed line), the lower-order model with four poles ($p_{1,2}, p_{3,4}$) and two zeros ($z_{1,2}$) (see Table I) matches well the experimental frequency response in magnitude, but has a large modeling error in the phase (over 20°). By adding one pair of zeros (z_3 and z_4) and one pair of poles (p_5 and p_6) at relatively-high frequencies, the phase error in the model is removed without affecting the magnitude response in the modeled frequency range. The frequency response of the model we used, $\hat{G}(s)$, with the phase compensation, matches the experimentally measured magnitude and phase response well up to 1 KHz (see Fig. 3).

State Space Model A minimal state-space realization of the transfer function $\hat{G}(s)$ in Eq. (2) can be obtained as

$$\dot{x}(t) = Ax(t) + Bu(t) \quad (3)$$
$$y(t) = Cx(t) \quad (4)$$

where $x(t) \in \Re^6$ is the state, $u(t),\ y(t) \in \Re$ are the input and output respectively and

$$A = \begin{bmatrix} -0.110 & 3.189 & 0.085 & 0 & 0 & 0 \\ -3.189 & -0.110 & -2.486 & 0 & -0.006 & 0 \\ 0 & 0 & -0.121 & 5.699 & 0.422 & 0 \\ 0 & 0 & -1.425 & -0.121 & 3.480 & 0 \\ 0 & 0 & 0 & 0 & -11.938 & 4.000 \\ 0 & 0 & 0 & 0 & 0 & -11.938 \end{bmatrix}$$
$$B = \begin{bmatrix} 0 & 0 & 0 & 0 & 0 & 3.729 \end{bmatrix}^T,$$
$$C = \begin{bmatrix} 1.330 & 0 & 6.501 & 0 & 0.015 & 0 \end{bmatrix} \quad (5)$$

B. Precision Positioning: Inversion-Based Approach

Inversion-based approach has been applied to various applications (see, e.g., [17-20], for a few). Next, we describe the inversion process for the experimental inertial reaction device.

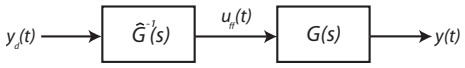

Fig. 4. Feedforward inversion-based control inverts the system model $\hat{G}(s)$ to produce exact tracking of the desired trajectory $y_d(t)$.

The inverse input $u_{ff}(t)$ Next we outline the inverse process to obtain the feedforward $u_{ff}(t)$ by using the state-space model (3, 4). Such inverse feedforward input $u_{ff}(t)$, when applied to the system (see Fig. 4), can achieve exact output tracking of the driving waveform, i.e., the precision positioning of the piezo actuator. We find the inverse input by differentiating the output (3) and substituting in the state-dynamics Eq. (4) till the input appears explicitly in the expression. The number of differentiation needed (till the input appears) depends on the relative degree (e.g., [20]) of the system (which is the difference between the number of poles and the number of zeros for a single-input single-output system). The piezo actuator model (3, 4) has relative degree of 2 (Eq. (2)), differentiating the output $y(t)$ twice leads to

$$\ddot{y}(t) = CA^2x(t) + CABu_{ff}(t), \quad (6)$$

and the inverse input $u_{ff}(t)$ is obtained from Eq. (6) as

$$u_{ff}(t) = -(CAB)^{-1}CA^2x(t) + (CAB)^{-1}\ddot{y}_d(t) \quad (7)$$

Equation (7) shows that to find the exact output-tracking inverse input $u_{ff}(t)$, the state trajectory $x(t)$ needs to be specified. Such state is called *the reference state*, $x_{ref}(t)$, which is found by solving the internal dynamics [20] of the system for the given desired trajectory $y_d(t)$. To find the internal dynamics, we define the following state transformation

$$\begin{bmatrix} \xi(t) \\ \eta(t) \end{bmatrix} = Tx(t) \quad (8)$$

where $\xi(t)$ is the output and its derivative, $\xi(t) = [y(t),\ \dot{y}(t)]^T$, $\eta(t) = [\eta_1(t),\ \eta_2(t),\ \eta_3(t),\ \eta_4(t)]^T$ and the mapping matrix $T : \Re^6 \to \Re^6$ is invertible. Then the internal dynamics is found by rewriting the state Eq. (3) in the $[\xi,\ \eta]^T$ coordinate and substituting in the inverse input $u_{ff}(t)$ (Eq. (7)),

$$\dot{\eta}(t) = A_\eta\eta(t) + B_\eta Y_d(t) \quad (9)$$

where $Y_d(t) = [\xi_d(t),\ y_d^{(3)}(t)]^T$ (see, e.g., [20] for a detailed description of the inversion process for general linear time invariant system). Therefore, Equations (7, 9) show that finding a bounded inverse input $u_{ff}(t)$ is equivalent to finding a bounded solution of the internal dynamics (9). Since the eigenvalues of the internal dynamics mapping A_η are the zeros of the system (3, 4) (e.g., [20]), and

system (3, 4) has four minimum-phase zeros, the internal dynamics (9) is stable. Therefore, the bounded solution to the internal dynamics (9) can be found by flowing the state forward in time, i.e., the internal dynamics can be obtained online from the measured state trajectory via state transformation (8). For nonminimum-phase system, online implementation of the inverse process can be realized if the *preview* information of the desired trajectory is available, see [13] for detail.

Remark 1: The inverse input, when applied as a feedforward input, leads to exact tracking of the desired driving waveform provided the model is perfect. However, most models tend to have uncertainties, particularly at high frequencies. For example, in this application, the system is only modeled till 1 KHz and can have large modeling errors at higher frequencies. In such cases, the inversion scheme can be modified to only invert the vibration dynamics in the frequency range where the modeling errors are small, for example, by using the optimal inversion approach [12], [17]. Furthermore, the acceptable modeling error in using the inversion-based approach to improve the tracking performance is quantified in [21].

III. Results and Discussion

The feedforward inverse input $u_{ff}(t)$ found in Section II-B is applied in both simulation and experiment to track the driving waveform. The results are compared with those obtained by using the *DC-Gain* approach to show the efficacy of the proposed method in achieving high-speed high-precision positioning of the piezo actuator, which improves the operation speed of the inertial reaction device.

A. Choice of Driving Waveforms

In this paper, a sawtooth driving waveform is chosen (see Fig. 1 (a), (b)) as in previous works (e.g., [1], [2], [5], [7], [8]). We note that considerable research effort has focused on the choice of the driving waveform to increase the operation speed of inertial reaction devices. For example, parabolic waveforms (e.g., [6]) , cycloidal waveforms [3] and hybrid waveforms consisting of sawtooth and parabolic waveform [22] have been proposed. Although the use of these *redesigned* waveforms has shown some improvement in the high-speed operation of inertial reaction devices, their success is quite limited since the dynamics of the piezo actuator is not explicitly accounted for in designing the input used to track these waveforms through the actuator.

The proposed inversion-based method tracks the driving waveform exactly– regardless the type of waveform– therefore, it can be applied to improve the operation speed of the inertial reaction device even when other waveforms are employed.

Remark 2: Inversion-based approach finds the *unique* inverse input to achieve exact output tracking for linear time invariant, provided the desired trajectory is bounded till r^{th} (r is the relative degree of the system) order of its derivatives (see Eq. (7)). In this experiment, it requires that the sawtooth and its twice derivatives, $y_d(t), \dot{y}_d(t), \ddot{y}_d(t)$, to be bounded (see Eq. (7). Therefore, the sawtooth trajectory is numerically filtered to smooth out the turn-around corners in the trajectory. The cut-off frequency of the filter is set at $f_{filt} = 500\ (Hz)$, which is close to the dominant resonant peak of the system's actuators at 508 Hz. This cut-off was chosen for two reasons: (1) tracking frequency components higher than the resonant peak requires large input amplitude (due to the drop of the system's gain (see Fig. 3)), which may lead to actuator saturation; (2) the modeling error increases at frequencies higher than resonance because of the decreased signal-to-noise ratio, generating increased error in computing the inverse input, thereby increased tracking error.

B. Improvement of the Piezo Actuator Output Tracking

Simulation study: Inversion-based method achieves precision positioning at high waveform frequency. We compare the tracking performance using the inversion-based method with using the *DC-Gain* method for the sawtooth waveform desired trajectory at (1) low frequency (50 Hz) and (2) high frequency (200 Hz). The inputs obtained in simulation by using the *DC-Gain* method and the inversion-based approach are compared in Fig. 5 (a)) (50 Hz) and plot (c) (200 Hz), and the corresponding output tracking achieved in simulation are also compared in Fig. 5 for 50 Hz (plot (b)) and 200 Hz (plot(d)). At low waveform frequency 50 Hz, the variations of the actuator dynamics (magnitude and phase of the frequency response) are small (see Fig. 3), therefore the dynamics effect of the piezo actuator is not significant. Consequently, the input obtained from the *DC-Gain* method is close to the inverse input $u_{ff}(t)$, as shown in Fig. 5 (a), and reasonably good output tracking can be achieved by using the *DC-Gain* method (see Fig. 5 (b)). However, as the waveform frequency increases, the variations of actuator dynamics become large (see Fig. 3). Therefore, the *DC-Gain* approach, which does not account for those variations in computing the input, cannot track the desired waveform and large tracking error occurs, as shown in Fig. 5 (d) for the waveform frequency of 200 Hz. By accounting for the frequency-dependent magnitude and phase variations in generating the inverse input, the inversion-approach achieved exact output tracking in simulation (see Fig. 5 (d)). Note the large difference between the *DC-Gain* input and the inverse input when the waveform frequency is high (200 Hz) in Fig. 5 (c) — this difference indicates that the inverse input accounts for the actuator dynamics.

C. Experimental Results

To verify the predicted improvement in system performance, the vibration compensation technique was applied to the inertial-reaction device described in section II-A (Fig. 2). The actual response of the systems actuators, for both the *DC-gain* and inversion-based control inputs

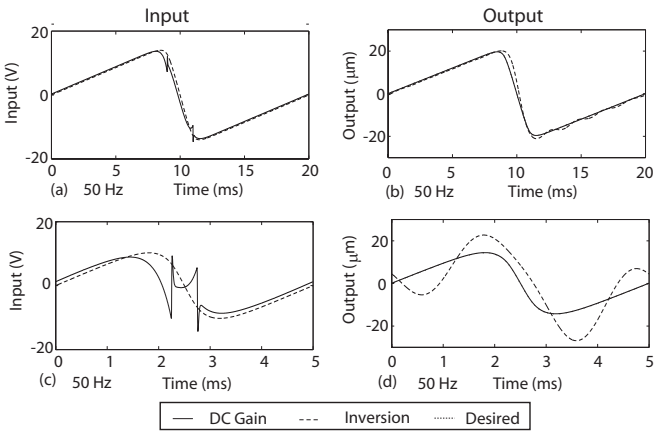

Fig. 5. Simulated response of the piezo actuator for a relatively low frequency driving waveform ($50\ Hz$, (a) input, and (b) output) and a high frequency driving waveform ($200\ Hz$, (c) input, and (d) output).

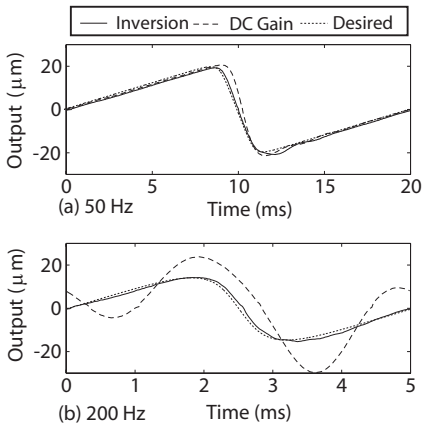

Fig. 6. Experimental tracking results of the desired waveform for frequency of $50\ Hz$ (a) and $200\ Hz$ (b), by using the *DC-Gain* method (dashed-line) and the inversion-based approach (solid-line).

were recorded.

Experimental Study: Inversion-based method significantly improves the actuator tracking of high-frequency driving waveform. The displacement of the system's actuators was measured using an inductive sensor. Fig. 6 shows the response of the piezoceramic actuator and Fig. 7 the tracking error, for the same two driving waveform frequencies used in simulation (50 and 200 Hz). As predicted by the simulation for the waveform frequency significantly below system resonance ($f = 50$ Hz) both the DC-gain (dashed-line) and inversion-based (solid-line) control strategies track the desired trajectory (dotted-line) well (Fig. 6a and Fig. 7a). For a sufficiently high driving frequency ($f = 200$ Hz), however, the DC-gain approach (dashed-line) induces vibrations in the actuator whereas the inversion-based control scheme (solid-line) continues to track the desired trajectory (dotted-line) without significant vibrations (Fig. 6b and Fig. 7b).

Notice that for both the low and high frequency driving waveforms, Fig. 6 shows that the inversion-based control output (solid-line) varies slightly from the desired trajectory (dotted-line) (also see Fig. 7). These small variations are most likely due to the errors in the system model (2) from unmodeled nonlinear dynamics effects (such as creep and hysteresis) and system disturbances. Although small tracking errors are present, the inversion-based control approach results in a substantial tracking improvement, particularly at at high frequency driving waveform. When the driving waveform frequency is 200 Hz, the maximum tracking error is reduced more than 90% (from $17.4\ \mu m$ to $1.6\ \mu m$) by using the proposed inversion-based approach. Therefore, the inversion-based approach can significantly improve the tracking performance of the driving waveform at high frequency. In the next section we investigate how this vibration compensation affects the operating speed of the inertial reaction device.

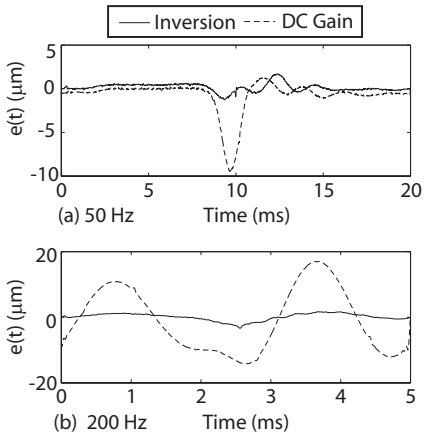

Fig. 7. Experimental Tracking error of the desired waveform for frequency of $50\ Hz$ (a) and $200\ Hz$ (b), by using the *DC-Gain* method (dashed-line) and the inversion-based approach (solid-line).

Experimental study: Inversion-based approach more than doubled the angular velocity of the inertial reaction device. Angular velocity of the inertial-reaction rotational motor (Fig. 2) was measured using a quadrature optical encoder. Multiple measurements ($N = 150$) were averaged and the sample mean of the rotational speed is presented in Fig. 8 for a variety of waveform frequencies; for every case the sample standard deviation obtained was less than $0.01\ (rad/s)$. However, speeds below $0.035\ (rad/s)$ could not be measured because of time constraints; it took too long to record enough measurements for a reliable sample mean and standard deviation. Therefore for any measurements below this threshold the mean was set to zero.

At low frequencies ($30 - 60\ Hz$), the *DC-gain* and inversion-based control schemes show similar performance since the waveform frequencies are sufficiently below the system's resonance frequency and unwanted vibrations are not excited. This agrees with our simulation results (Fig. 6a) which predict that both the *DC-gain* and the inversion-based control approaches result in reasonable tracking of the desired sawtooth trajectory (which should result in the

desired slip and stick motion). However, substantial performance degradation is observed, at higher driving waveform frequencies ($> 60\ Hz$), if the system dynamics is not accounted for. For example, the system's rotational speed (with DC-gain control) decreases for frequencies between $80 - 120\ (Hz)$ at which point the speed is almost zero (Fig. 8). Continuing to increase the driving waveform frequency also results in rotation in the opposite direction (see $f = 130, 160 - 200\ Hz$ in Fig. 8). In contrast, for the inversion-based control scheme, the rotational speed continues to increase since the actuator continues to track the desired sawtooth driving waveform. As seen in Fig. 8 the maximum speed reached using the *DC-gain* control scheme is $0.18\ (rad/s)$ at a driving waveform frequency of $80\ (Hz)$, whereas the maximum speed for the inversion-based control scheme is $0.42\ (rad/s)$ at a frequency of $180\ (Hz)$, more than twice as fast. Thus, the inversion-based control strategy significantly improves the speed of the inertial reaction device.

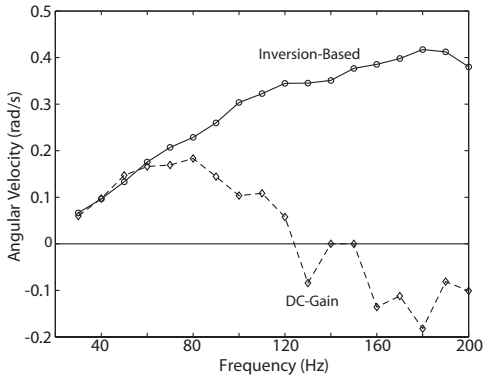

Fig. 8. Angular speed of the inertial-reaction device at 18 different frequencies for both *DC-gain* (dashed-line, diamonds) and inversion-based (solid-line, circles) control. The sample mean was calculated for each case from 150 measurements. The standard deviation was less than $0.01\ (rad/s)$ for each frequency measured.

IV. Conclusions

Inversion-based control was used to improve the operation of an inertial reaction device. The technique inverts a model of the actuator dynamics to find inputs that track the desired trajectory. Compared with the standard *DC-gain* control approach, vibrations in the actuator induced at high driving waveform frequencies are substantially reduced using the inversion-based control. Better tracking of the desired driving waveform of high frequency results in more than doubling of the operating speed.

V. Acknowledgments

The authors wish to thank Joseph Garbini and Paul Labossiere both of the University of Washington, Don Croft of Raytheon, and the Mechanical Engineering senior design project group of 2001 for the design and manufacture of the inertial reaction device utilized in this article. This work was partly supported by NASA Ames Research Grant NAG 2-1450.

References

[1] D. W. Pohl, "Dynamic piezoelectric translation devices," *Rev. Sci. Instrum.*, vol. 58, pp. 54–57, Jan. 1987.

[2] P. Niedermann, R. Emch, and P. Descouts, "Simple piezoelectric translation device," *Rev. Sci. Instrum.*, vol. 59, pp. 368–369, Feb. 1988.

[3] C. Renner, P. Niedermann, A. D. Kent, and O. Fischer, "A vertical piezoelectric inertial slider," *Rev. Sci. Instrum.*, vol. 61, pp. 965–967, Mar. 1990.

[4] B. L. Blackford, "A simple self-propelled two-dimensional micropositioner," *Rev. Sci. Instrum.*, vol. 64, pp. 1360–1361, May 1993.

[5] J. Tapson and J. R. Greene, "A simple dynamic piezoelectric x-y translation stage suitable for scanning probe microscopes," *Rev. Sci. Instrum.*, vol. 64, pp. 2387–2388, Aug. 1993.

[6] L. Libioulle, A. Ronda, I. Derycke, J. P. Vigneron, and J. M. Gilles, "Vertical two-dimensional piezoelectric inertial slider for scanning tunneling microscope," *Rev. Sci. Instrum.*, vol. 64, pp. 1489–1494, Jun. 1993.

[7] L. Howald, H. Rudin, and H.-J. Guntherodt, "Piezoelectric inertial stepping motor with spherical rotor," *Rev. Sci. Instrum.*, vol. 63, pp. 3909–3912, Aug. 1992.

[8] R. T. Brockenbrough and J. W. Lyding, "Inertial tip translator for a scanning tunneling microscope," *Rev. Sci. Instrum.*, vol. 64, pp. 2225–2228, Aug. 1993.

[9] W. Zesch, R. Buchi, C. Alain, and R. Siegwart, "Inertial drives for micro- and nanorobots: Two novel mechanisms," *Proceedings of SPIE*, vol. 2593, pp. 80–88, Oct. 1995.

[10] J. M. Breguet and R. Clavel, "Stick and slip actuators: design, control, performances and applications," in *Proceedings: International Symposium on Micromechatronics and Human Science*, pp. 89–95, 1998.

[11] S. Devasia, D. Chen, and B. Paden, "Nonlinear inversion-based output tracking," *IEEE Trans. on Automatic Control*, vol. 41, no. 7, pp. 930–942, 1996.

[12] J. S. Dewey, K. Leang, and S. Devasia, "Experimental and theoretical results in output-trajectory redesign for flexible structures," *ASME Journal of Dynamic Systems, Measurement and Control*, vol. 120, pp. 456–461, Dec. 98.

[13] Q. Zou and S. Devasia, "Preview-based stable-inversion for output tracking of linear systems," *ASME Journal of Dynamic Systems, Measurement and Control*, vol. 121, pp. 625–630, Dec. 1999.

[14] R. L. Clark, "Accounting for out-of-bandwidth modes in the assumed modes approach: Implications on colocated output feedback control," *ASME Journal of Dynamic Systems, Measurement and Control*, vol. 119, pp. 390–395, September, 1997.

[15] S. O. R. Moheimani, "Minimizing the effect of out of bandwidth modes in truncated structure models," *ASME Journal of Dynamic Systems, Measurement and Control*, vol. 122, pp. 237–239, March, 2000.

[16] D. Croft, G. Shedd, and S. Devasia, "Creep, hysteresis, and vibration compensation for piezoactuators: Atomic force microscopy application," *ASME Journal of Dynamic Systems, Measurement and Control*, vol. 123(35), pp. 35–43, March, 2001.

[17] Q. Zou and S. Devasia, "Preview-based optimal inversion for output tracking: Application to scanning tunneling microscopy," *IEEE Trans. on Control Systems Technology*. accepted.

[18] E. Bayo, "A finite-element approach to control the end-point motion of a single-link flexible robot," *Journal of Robotic Systems*, vol. 4, no. 1, pp. 63–75, 1987.

[19] L. R. Hunt, G. Meyer, and R. Su, "Noncausal inverses for linear systems," *IEEE Trans. on Automatic Control*, vol. 41, no. 4, pp. 608–611, 1996.

[20] A. Isidori, *Nonlinear Control Systems*. London: Springer-Verlag, third ed., 1995.

[21] S. Devasia, "Should model-based inverse input be used as feedforward under plant uncertainty?," *IEEE Trans. on Automatic Control*, vol. 47, pp. 1865–1871, Nov. 2002.

[22] C. N. Woodburn, A. W. McKinnon, D. A. Roberts, M. E. Taylor, and M. E. Welland, "A one-dimensional piezoelectric-driven inertial micropositioner with vertical capabilities," *Meas. Sci. Technol.*, vol. 4, no. 4, pp. 535–537, 1993.